Phenylglycine Amphiphile-Metal Ion Chiral Supramolecular Nanozymes for Enantioselective Catalysis

Dongying Li,[a†] Cong Gao, [a†] Cici Zhao, Qingqing Sun,[a*] Zheng Xi,[a*] Jie Han[a*] and Rong Guo[a]

[a]Yangzhou University, School of Chemistry and Chemical Engineering, Yangzhou, 225002 Jiangsu, China.

[†]These authors contributed equally.

Supporting Information

Table of Contents

1. Experimental Section

Materials

L- and D- phenylglycine (L-/D-Phg), palmitoyl chloride sodium bicarbonate ($NaHCO_3$), sodium hydroxide (NaOH), hydrochloric acid (HCl), tetrahydrofuran (THF), 3, 4-dihydroxy-L-phenylalanine (L-DOPA) and 3,4-dihydroxy-D-phenylalanine (D-DOPA) were purchased from Sigma-Aldrich. Copper nitrate trihydrate ($Cu(NO_3)_2{\cdot}3H_2O$), cobalt chloride hexahydrate ($CoCl_2{\cdot}6H_2O$), manganese chloride tetrahydrate ($MnCl_2{\cdot}4H_2O$), zinc Chloride ($ZnCl_2$) were obtained from Shanghai Macklin Biochemical Co., Ltd. (Shanghai, China). Hydrogen peroxide (H_2O_2) were obtained from Sinopharm Chemical Reagent Co., Ltd. (Shanghai, China). All the above reagents were of analytical grade and used without further purification. The water used in this study was deionized by Milli-Q Plus system (Millipore, France), having 18.2 MΩ electrical resistivity.

Synthesis of L- and D-PhgC$_{16}$

L-PhgC$_{16}$ was prepared according to a similar procedure previously reported in the literature.[1] L-phenylglycine (0.15 g, 1 mmol) was dissolved in the mixture of aqueous 1 M NaOH (1.3 mL), 10% $NaHCO_3$ (1.1 mL) and THF (1 mL). A solution of palmitoyl chloride in THF was added dropwise to the above solution, and the mixture was stirred for 3 h at 0 ℃. After that, THF was evaporated and the remaining solution was acidified with 2 M HCl, and extracted with CH_2Cl_2 (x 3). The crude product was recrystallized with hexane to afford the product as a white solid (223 mg, 60% yield). **D-PhgC$_{16}$** was also synthesized according to the above method.

Preparation of (*P*)-D-PhgC$_{16}$-NR-M(II) and (*M*)-L-PhgC$_{16}$-NR-M(II)

D-PhgC$_{16}$ or L-PhgC$_{16}$ (4.67 mg, 0.012 mmol) was dissolved in methanol (1.5 mL) in a 10 mL flask. Then, water (2.5 mL) was added to the solution and the reaction mixture was allowed to stirring for 10 min at r.t. to afford the supramolecular assemblies, **(*P*)-D-PhgC$_{16}$-NR** or **(*M*)-L-PhgC$_{16}$-NR**. Separate solutions of $CoCl_2$ (1 M), $CuCl_2$ (0.1 M), $MnCl_2$ (0.05 M), and $ZnCl_2$ (0.025 M) were prepared in water, and then added to the aqueous solution of the as prepared **(*P*)-D-PhgC$_{16}$-NR**, respectively. The solution mixtures were stirred for 10 min to give the metal coordinated chiral assembly, **(*P*)-D-PhgC$_{16}$-NR-M(II)**. The **(*M*)-L-PhgC$_{16}$-NR-M(II)** counterpart was also synthesized according to the above method.

Measurements and characterizations

The ^{1}H-NMR and ^{13}C NMR analysis were performed on the NMR spectrometer (Quantum-I plus 600 MHz, Q. One Instruments Ltd., China). The AFM experiments were carried out on a Multimode 8 Scanning Force Microscope (Bruker). Bruker AFM cantilevers for the tapping mode in soft tapping conditions were used at a vibrating frequency of 150 kHz. Images were simply flattened using the Nanoscope 8.1 software, and no further image processing was carried out. The critical aggregation concentration analysis was conducted on a DDSJ-308A Conductivity Meters.

The FTIR spectra were recorded using a JASCO model FT/IR-6100Plus FT-IR spectrometer. For the monomer, D-PhgC$_{16}$, the IR experiment was done in solid state (KBr as the reference). Supramolecular assemblies of **(*P*)-D-PhgC$_{16}$-NR-M(II)** were first prepared in a solvent mixture of 4/6 methanol/water. Centrifuge the solution and mix the residue with solid KBr to form a disc for analyzing.

X-ray diffraction (XRD) was conducted on a D8 ADVANCE X-ray diffractometer. Supramolecular assemblies of **(*P*)-D-PhgC$_{16}$-NR** and **(*P*)-D-PhgC$_{16}$-NR-M(II)** were first prepared in a solvent mixture of 4/6 methanol/water. Centrifuge the solution and transfer the residue to a quartz glass piece. Prior to analysis, the components were

dried in ambient and freeze-drying conditions.

Circular dichroism (CD) analysis was performed on a JascoJ-810 CD spectropolarimeter (JASCO International Co., Ltd., Japan) with a resolution of 1 nm in the wavelength range of 205−300 nm. All the measured samples of CD spectra were performed in the 1 cm quartz cuvette. The measured samples of CD spectra for assembly and nanozymes were prepared in a methanol/water solvent mixture at a concentration of 0.15 mM. The L/D-DOPA concentration for the CD measurements is 50 μM, prepared in a 4/6 methanol/water mixture.

The UV-Vis absorption spectra were recorded using UV-2550 UV-Visible spectrophotometer (JASCO International Co., Ltd., Tokyo, Japan). Spectral measurements and kinetic measurements were performed in the 1 cm (4.5 mL) quartz cuvette.

The ICP-AES analysis were determined by Inductively Coupled Plasma-Atomic Emission Spectrometry (ICP-AES, Optima 7300 DV, PerkinElmer, US). Supramolecular assemblies of **(*P*)-D-PhgC$_{16}$-NR-M(II)** were first prepared in a solvent mixture of 4/6 methanol/water. The solution was centrifuged, and the supernatant was diluted and placed in a centrifuge tube for testing.

UV-vis titration experiments: A solution of **(*P*)-D-PhgC$_{16}$-NR** or **(*M*)-L-PhgC$_{16}$-NR** (133 μM) was prepared in a 4/6 methanol/water solvent mixture. Subsequently, 2.5 mL of the solution was placed in a quartz cuvette and the absorption spectrum was recorded. Separate solutions of $CoCl_2$, $CuCl_2$, $MnCl_2$, and $ZnCl_2$ with a concentration of 400 μM was prepared in water. The solution of **(*P*)-D-PhgC$_{16}$-NR** or **(*M*)-L-PhgC$_{16}$-NR** was titrated by adding incremental amounts of the metal ion solution and recording a UV-vis spectrum after each addition. The association constants were calculated by monitoring the absorbance changes at 218 nm after each addition.

Kinetic measurements

Kinetic measurements were conducted in a time-course mode by monitoring the absorbance changes at 475 nm. Experiments were performed using the as obtained **(*P*)-D-PhgC$_{16}$-NR-M(II)** or **(*M*)-L-PhgC$_{16}$-NR-M(II)** in a reaction volume of 3 mL (methanol/water, 4/6) with DOPA as substrate at 25 °C, and the concentration of H_2O_2 was kept constant at 50 mM. The concentration of DOPA in the catalytic oxidation process is in the range of 200-2000 μM. Initial rates were obtained from the slopes of the concentration vs time profiles in the kinetic runs following at least 30% of the reaction. Each measurement was repeated three times. Michaelis-Menten fitting of the V vs DOPA enantiomers plots were performed by the Origin software using the equation: $v = V_{max}C/(K_M+C)$, which afford the Michaelis constant K_M and the maximum reaction velocity V_{max}. In this equation, v is the initial velocity, which can be calculated according to Lambert Beer's law: $v = A\cdot\varepsilon^{-1}L^{-1}t^{-1}$, where A is the absorbance changes at λ_{max} = 475 nm (ε = 4770 $M^{-1}\cdot cm^{-1}$) of dopachrome products for D-DOPA and L-DOPA, L is the optical length of the used cuvette, and t is the time corresponding to the absorbance changes. V_{max} is the maximal reaction velocity, and C is the concentration of DOPA as substrate. Using K_{cat} to express the catalytic activity of enzymes, and $K_{cat} = V_{max}/S$, where S is the mass of the chiral nanozyme used in 1 mL reaction system. Select factor of various **(*P/M*)-D/L-PhgC$_{16}$-NR-M(II)** nanocatalysts for D-DOPA or L-DOPA was defined as $[K_{cat}/K_M]_{D\text{-}DOPA}/[K_{cat}/K_M]_{L\text{-}DOPA}$ or $[K_{cat}/K_M]_{L\text{-}DOPA}/[K_{cat}/K_M]_{D\text{-}DOPA}$, whichever larger than 1.

2. Synthesis of L- and D-PhgC$_{16}$

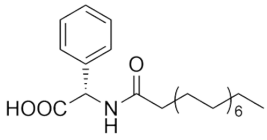

L-PhgC$_{16}$

Fig. S1. Line-drawing structure of **L-PhgC$_{16}$**.

^{1}H NMR ($CDCl_3$, 600 MHz): δ (ppm) = 7.41-7.31 (m, 5H), 6.52 (d, J = 6.8 Hz, 1H), 5.61 (d, J = 6.8 Hz, 1H), 2.29-2.24 (m, 2H), 1.60 (t, J = 7.2 Hz, 2H), 1.25 (s, 24H), 0.90 (t, J = 6.4 Hz, 3H).

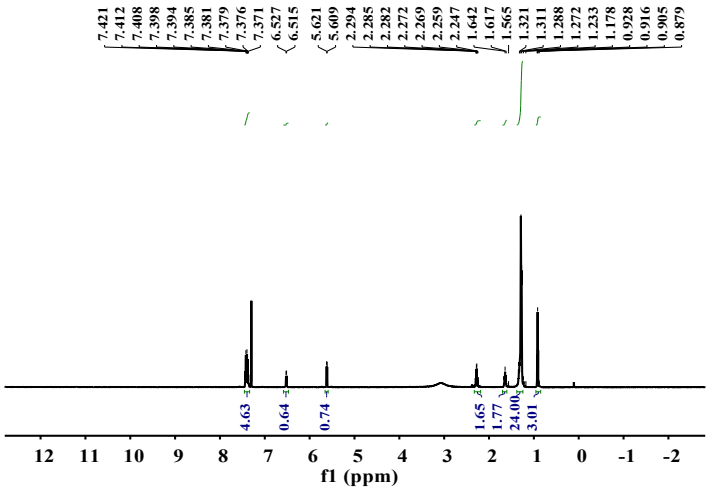

Fig. S2. ^{1}H NMR (600 MHz, $CDCl_3$, 298 K) spectrum of **L-PhgC$_{16}$**.

^{13}C NMR ($CDCl_3$, 150 MHz): δ (ppm) = 173.43, 173.35, 136.04, 129.22, 128.93, 127.54, 36.52, 32.09, 29.86-29.33, 25.63, 22.85, 14.28.

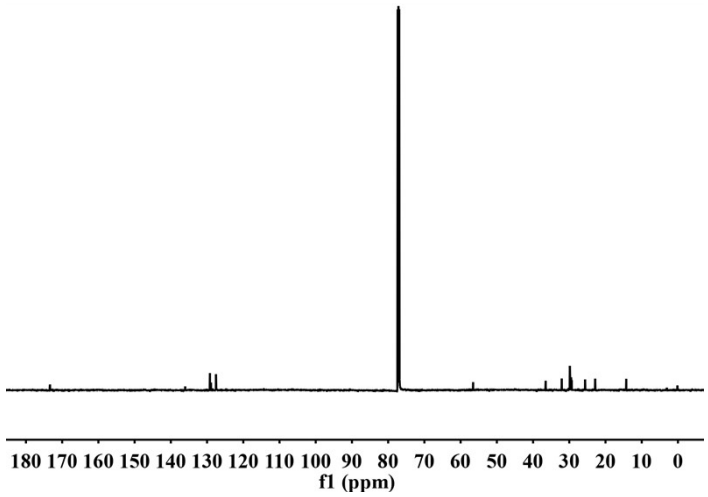

Fig. S3. ^{13}C NMR (150 MHz, $CDCl_3$, 298 K) spectrum of **L-PhgC$_{16}$**.

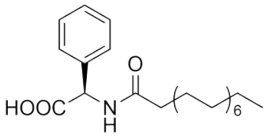

D-PhgC$_{16}$

Fig. S4. Line-drawing structure of **D-PhgC$_{16}$**.

^{1}H NMR ($CDCl_3$, 600 MHz): δ (ppm) = 7.42-7.36 (m, 5H), 6.44 (d, J = 6.8 Hz, 1H), 5.62 (d, J = 6.8 Hz, 1H), 2.28-2.22 (m, 2H), 1.63 (t, J = 7.2 Hz, 2H), 1.30 (s, 24H), 0.90 (t, J = 6.4 Hz, 3H).

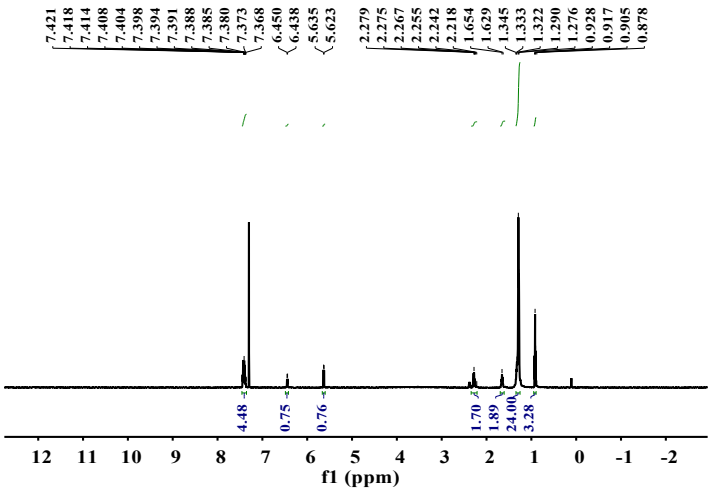

Fig. S5. ^{1}H NMR (600 MHz, $CDCl_3$, 298 K) spectrum of **D-PhgC$_{16}$**.

^{13}C NMR ($CDCl_3$, 600 MHz): δ (ppm) = 173.93, 173.56, 136.12, 129.17-128.86, 127.52, 36.50, 32.08, 29.86-29.32, 25.65, 22.85, 14.27.

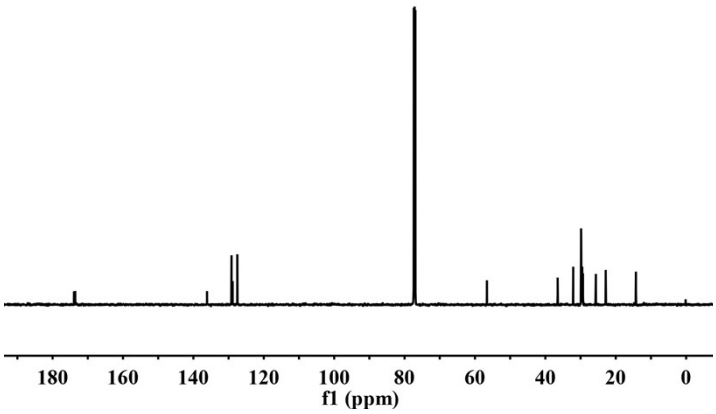

Fig. S6. ^{13}C NMR (150 MHz, $CDCl_3$, 298 K) spectrum of **D-PhgC$_{16}$**.

3. Characterizations of (*P*)-D-PhgC$_{16}$-NR-Co(II) and (*M*)-L-PhgC$_{16}$-NR-Co(II)

3.1 Critical aggregation concentration of amphiphile

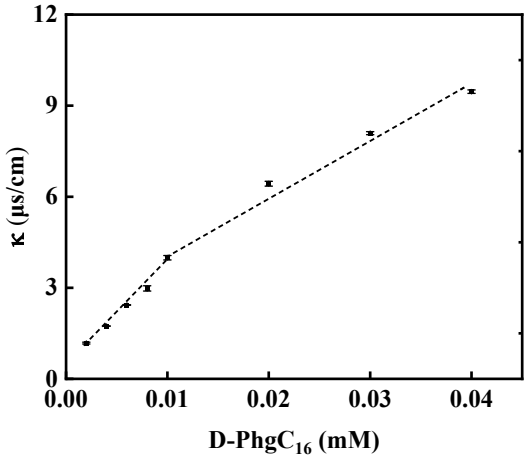

Fig. S7. Conductivity vs concentration of **D-PhgC$_{16}$** in a 4/6 methanol/water solvent mixture. The critical aggregation concentration (CAC) of **D-PhgC$_{16}$** was calculated to be 0.01 mM in this solvent mixture.

3.2 SEM images of (*P*)-D-PhgC$_{16}$-NR-Co(II) and (*M*)-L-PhgC$_{16}$-NR-Co(II)

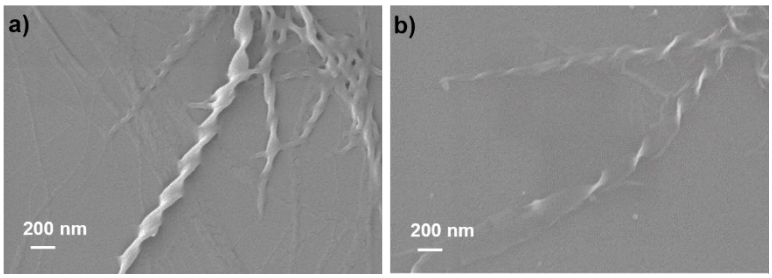

Fig. S8. SEM images of a) (*P*)-D-PhgC$_{16}$-NR-Co(II) and b) (*M*)-L-PhgC$_{16}$-NR-Co(II).

3.3 CD characterizations of (*P*)-D-PhgC$_{16}$-NR-Co(II)

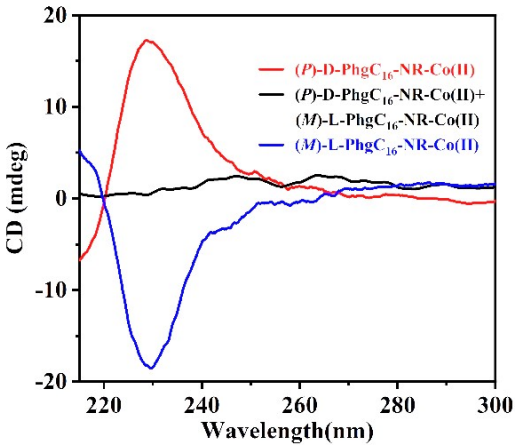

Fig. S9. CD spectra of (*P*)-D-PhgC$_{16}$-NR-Co(II), (*M*)-L-PhgC$_{16}$-NR-Co(II) and their equal molar mixtures.

3.4 XRD patterns of (*P*)-D-PhgC$_{16}$-NR-Co(II)

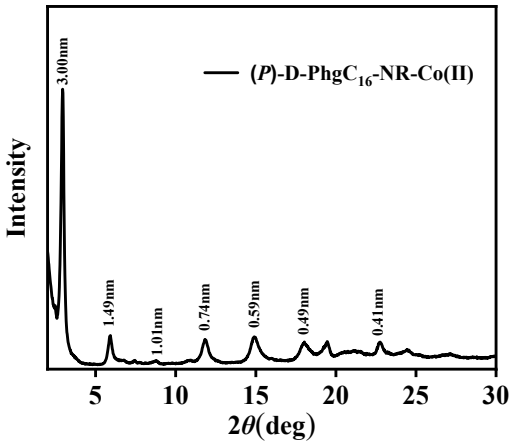

Fig S10. XRD patterns of **(*P*)-D-PhgC$_{16}$-NR-Co(II)**, which was prepared using freeze-drying method.

3.5 FTIR spectra of (*P*)-D-PhgC$_{16}$-NR-Co(II)

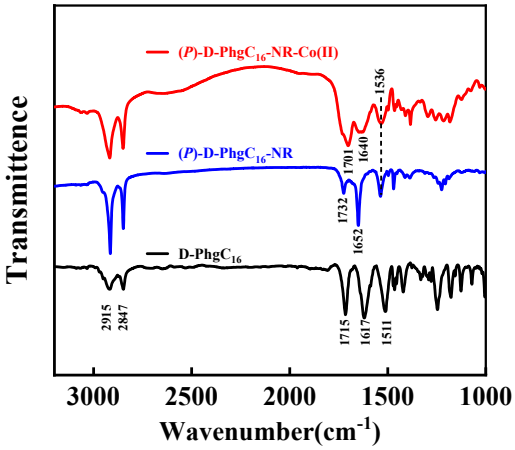

Fig. S11. FTIR spectra of **D-PhgC$_{16}$** (black line), **(*P*)-D-PhgC$_{16}$-NR** (blue line) and **(*P*)-D-PhgC$_{16}$-NR-Co(II)** (red line).

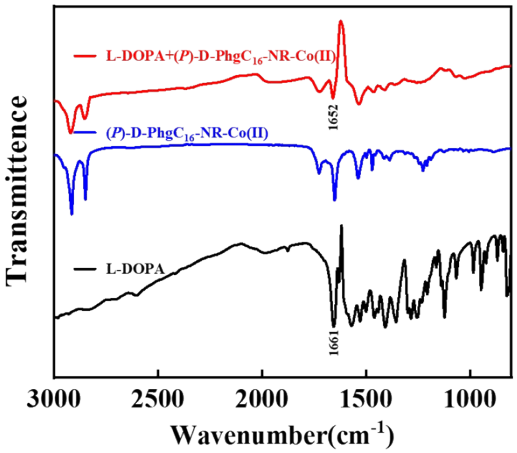

Fig. S12. FTIR spectra of **L-DOPA** (black line), **(*P*)-D-PhgC$_{16}$-NR-Co(II)** (blue line) and **L-DOPA+(*P*)-D-PhgC$_{16}$-NR-Co(II)** (red line).

3.6 Characterizations of (*P*)-D-PhgC$_{16}$-NR-M(II)

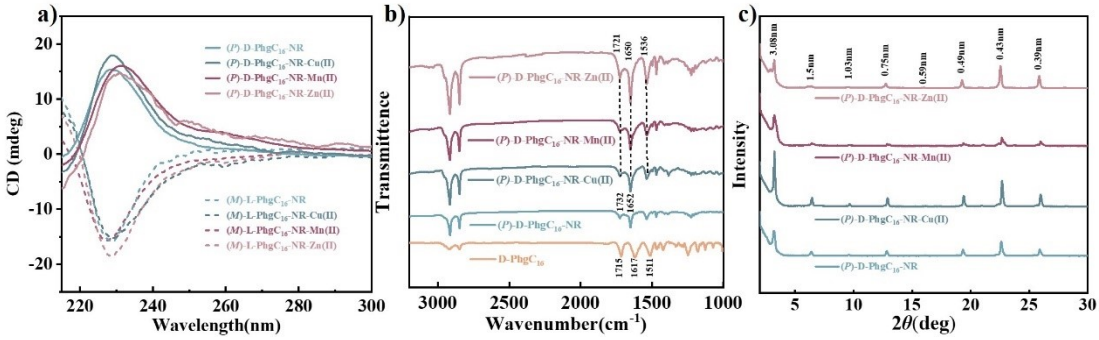

Fig. S13. a) CD spectra of supramolecular assemblies of **(*P/M*)-D/L-PhgC$_{16}$-NR** and **(*P/M*)-D/L-PhgC$_{16}$-NR-M(II)** (M = Cu, Mn and Zn) in 4/6 methanol/water solvent mixture. b) FTIR spectra of **D-PhgC$_{16}$, (*P*)-D-PhgC$_{16}$-NR** and **(*P*)-D-PhgC$_{16}$-NR-M(II)** (M = Cu, Mn and Zn). c) XRD patterns of **(*P*)-D-PhgC$_{16}$-NR** and **(*P*)-D-PhgC$_{16}$-NR-M(II)** (M = Cu, Mn and Zn). Inset: selected magnified XRD pattern.

3.7 Metal atomic analysis

Table S1. The M(II) concentration analysis before and after **(*P*)-D-PhgC$_{16}$-NR and (*M*)-L-PhgC$_{16}$-NR** adsorption through ICP-AES analysis.

Sample	M(II) concentration before absorption (mg·L^{-1})	M(II) concentration after absorption (mg·L^{-1})	M(II) concentration of absorption(mg·L^{-1})	Percentage of loaded ions added (%, mass percentage)	Percentage of loaded ions added (%, molar percentage)
(*P*)-D-PhgC$_{16}$-NR-Co(II)	59.00	25.96	33.04	**2.08**	**14.0**
(*M*)-L-PhgC$_{16}$-NR-Co(II)	59.00	26.08	32.92	**2.07**	**14.0**
(*P*)-D-PhgC$_{16}$-NR-Cu(II)	6.40	3.34	3.06	**0.20**	**1.2**
(*M*)-L-PhgC$_{16}$-NR-Cu(II)	6.40	3.53	2.87	**0.18**	**1.1**
(*P*)-D-PhgC$_{16}$-NR-Mn(II)	2.75	0.13	2.62	**0.17**	**1.2**
(*M*)-L-PhgC$_{16}$-NR-Mn(II)	2.75	0.47	2.28	**0.15**	**1.0**
(*P*)-D-PhgC$_{16}$-NR-Zn(II)	1.64	0.97	0.67	**0.04**	**0.25**
(*M*)-L-PhgC$_{16}$-NR-Zn(II)	1.64	0.97	0.67	**0.04**	**0.25**
(*M*)-L-PhgC$_{16}$-NR-Zn(II)	2.46	2.61	0.67	**0.04**	**0.25**
(*M*)-L-PhgC$_{16}$-NR-Zn(II)	3.28	2.61	0.68	**0.04**	**0.25**

3.8 UV titration experiments for all the combinations of (*P/M*)-D/L-PhgC$_{16}$-NR and the metal salts

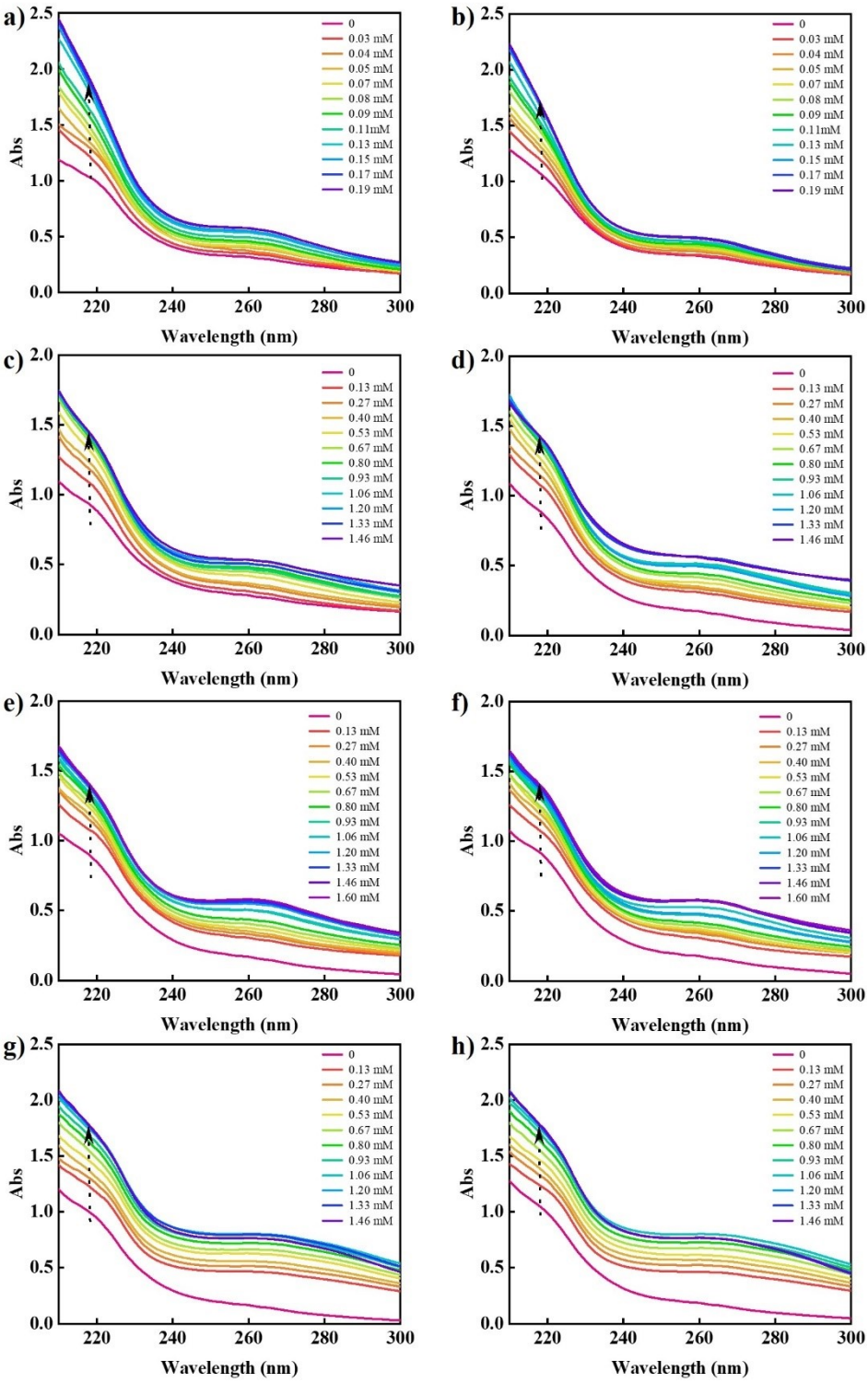

Fig. S14. a, c, e ,g) UV-vis titration spectra of **(*P*)-D-PhgC$_{16}$-NR** with the incremental addition of various metal ions; b, d, f ,h) UV-vis titration spectra of **(*M*)-L-PhgC$_{16}$-NR** with the incremental addition of various metal ions. (a, b) Co(II); (c, d) Cu(II), (e, f) Mn(II) and (g, h) Zn(II). The concentration of **(*P*)-D-PhgC$_{16}$-NR** or **(*M*)-L-PhgC$_{16}$-NR** was 133 μM.

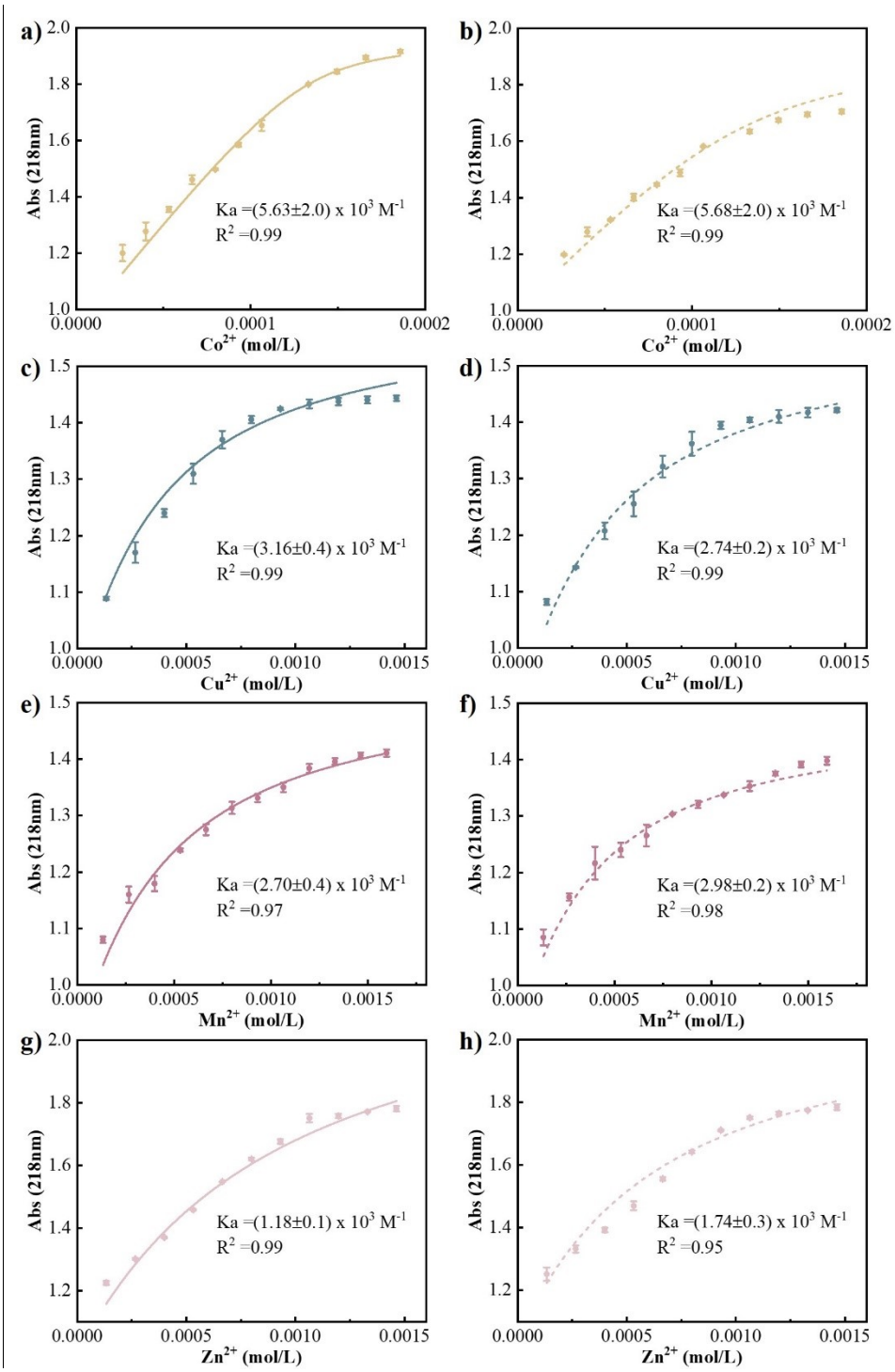

Fig. S15. a, c, e ,g) Fit of UV titration experiments for all the combinations of **(*P*)-D-PhgC$_{16}$-NR** and the metal ions; b, d, f ,h) Fit of UV titration experiments for all the combinations of **(*M*)-L-PhgC$_{16}$-NR** and the metal ions. (a, b) Co(II); (c, d) Cu(II), (e, f) Mn(II) and (g, h) Zn(II). The concentration of **(*P*)-D-PhgC$_{16}$-NR** or **(*M*)-L-PhgC$_{16}$-NR** was 133 μM.

Table S2. Association constants between the combinations of **(*P/M*)-D/L-PhgC$_{16}$-NR** and the metal salts.

Sample	Association constant (Ka, ×10³ M⁻¹)			
	Co(II)	Cu(II)	Mn(II)	Zn(II)
(*P*)-D-PhgC$_{16}$-NR	5.63±2.0	3.16±0.4	2.70±0.4	1.18±0.1
(*M*)-L-PhgC$_{16}$-NR	5.68±2.0	2.74±0.2	2.98±0.2	1.74±0.3

4. Kinetic experiments

4.1 Catalytic performance of (*P*)-D-PhgC$_{16}$-NR-Co(II) in different methanol/water solvent mixtures

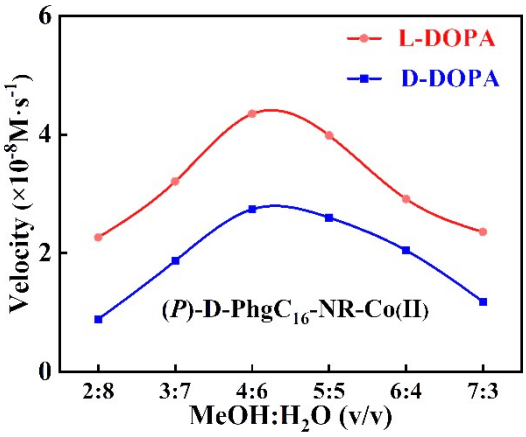

Fig. S16. Catalytic performance of **(*P*)-D-PhgC$_{16}$-NR-Co(II)** in different methanol/water solvent mixtures.

4.2 Catalytic performance of (*P*)-D-PhgC$_{16}$-NR-M(II) in the presence of different amounts of M(II)

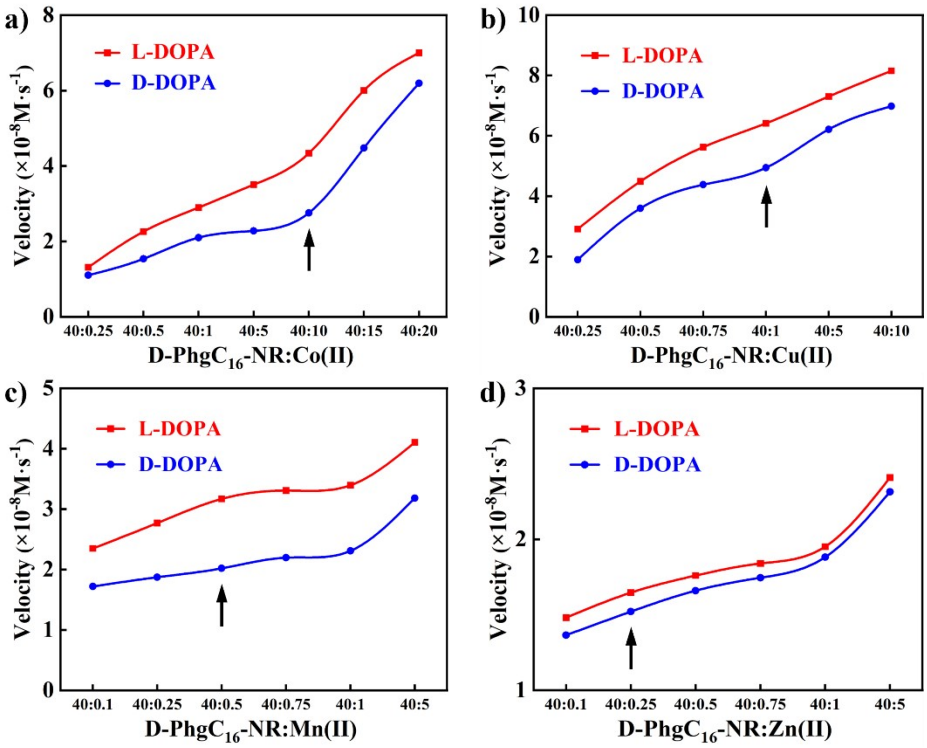

Fig. S17. Catalytic performance of **(*P*)-D-PhgC$_{16}$-NR-M(II)** in the presence of different amounts of M(II): a) Co(II); b) Cu(II); c) Mn(II) and d) Zn(II).

4.3 Time-dependent absorbance

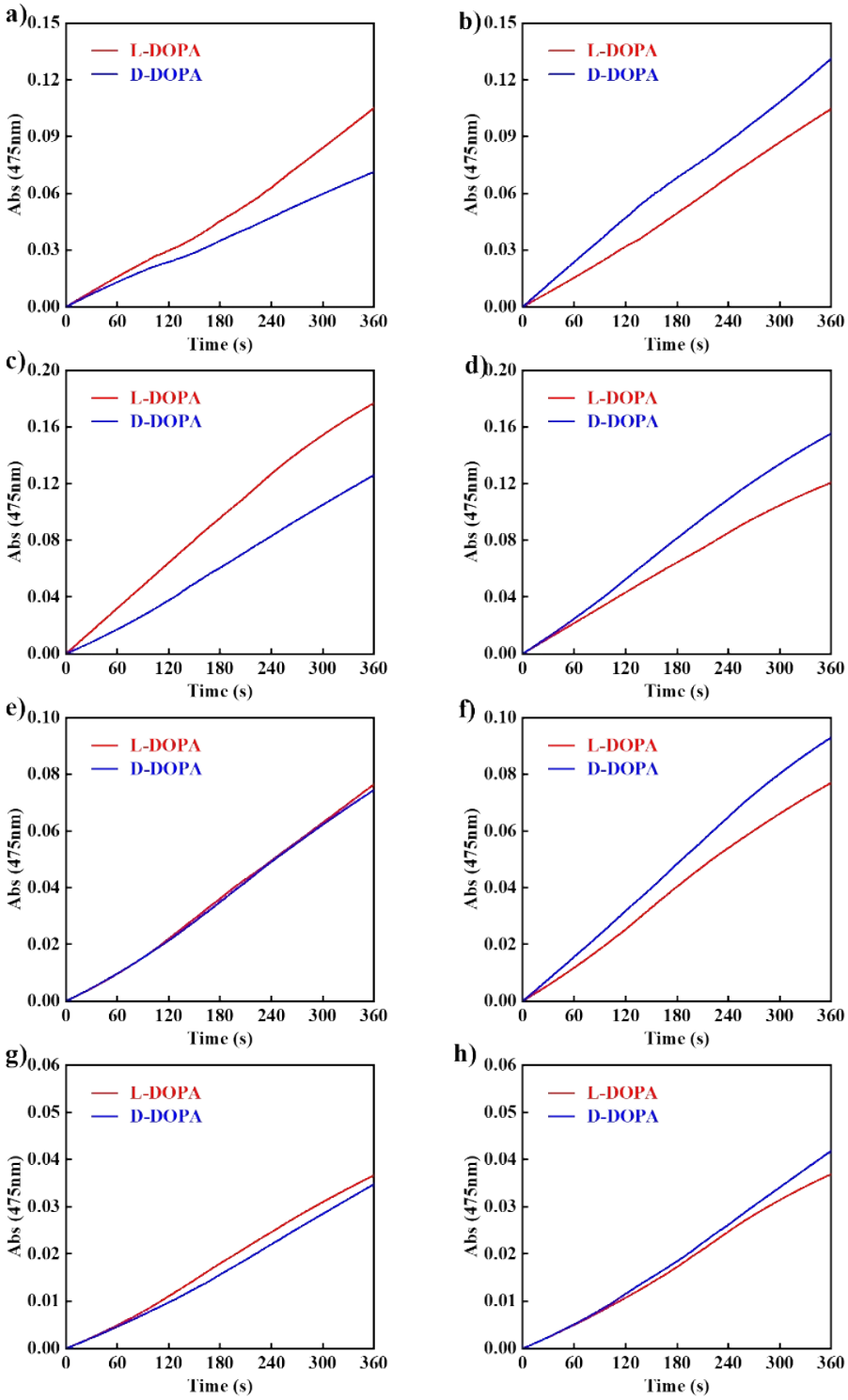

Fig. S18. The time-dependent absorbance at 475 nm using DOPA enantiomers as substrates and a) **(*P*)-D-PhgC$_{16}$-NR-Co(II);** c) **(*P*)-D-PhgC$_{16}$-NR-Cu(II);** e) **(*P*)-D-PhgC$_{16}$-NR-Mn (II);** g) **(*P*)-D-PhgC$_{16}$-NR-Zn(II);** b) **(*M*)-L-PhgC$_{16}$-NR-Co(II);** d) **(*M*)-L-PhgC$_{16}$-NR-Cu(II);** f) **(*M*)-L-PhgC$_{16}$-NR-Mn(II); and** h) **(*M*)-L-PhgC$_{16}$-NR-Zn(II)** as nanozymes. The concentration of L/D-DOPA is 2000 μM.

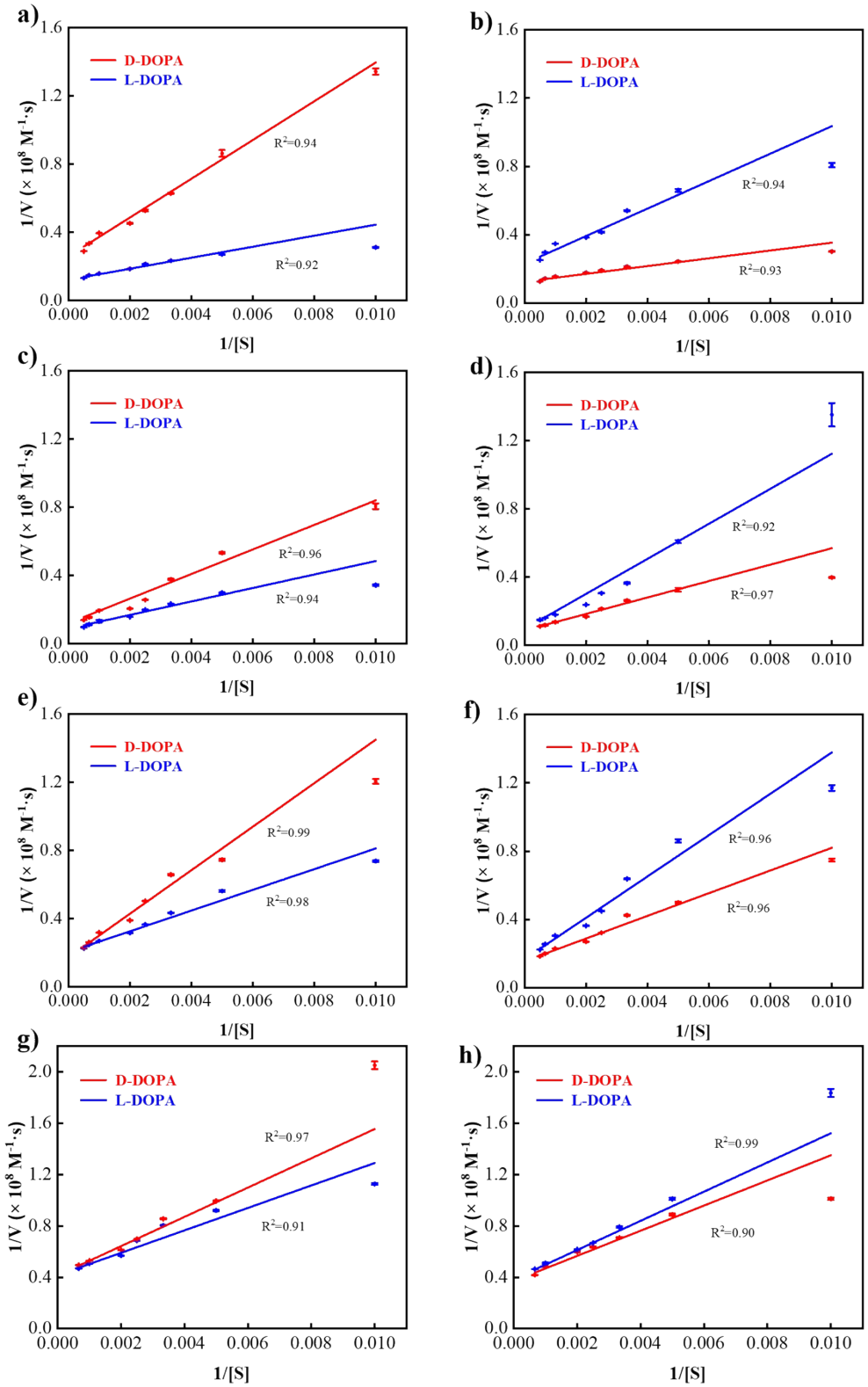

Fig. S19. Illustration by Lanewell-Burke showing the catalytic reactions towards D/L-DOPA for a) **(*P*)-D-PhgC$_{16}$-NR-Co(II);** c) **(*P*)-D-PhgC$_{16}$-NR-Cu(II);** e) **(*P*)-D-PhgC$_{16}$-NR-Mn (II);** g) **(*P*)-D-PhgC$_{16}$-NR-Zn(II);** b) **(*M*)-L-PhgC$_{16}$-NR-Co(II);** d) **(*M*)-L-PhgC$_{16}$-NR-Cu(II);** f) **(*M*)-L-PhgC$_{16}$-NR-Mn(II); and** h) **(*M*)-L-PhgC$_{16}$-NR-Zn(II).**

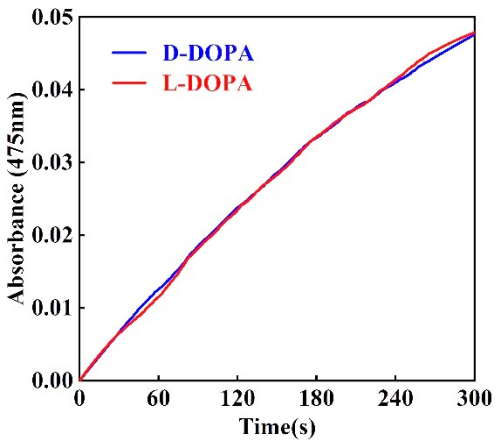

Fig. S20. Oxidation of D/L-DOPA enantiomers by equal molar amount of **(*P*)-D-PhgC$_{16}$-NR-Co(II)** and **(*M*)-L-PhgC$_{16}$-NR-Co(II)**.

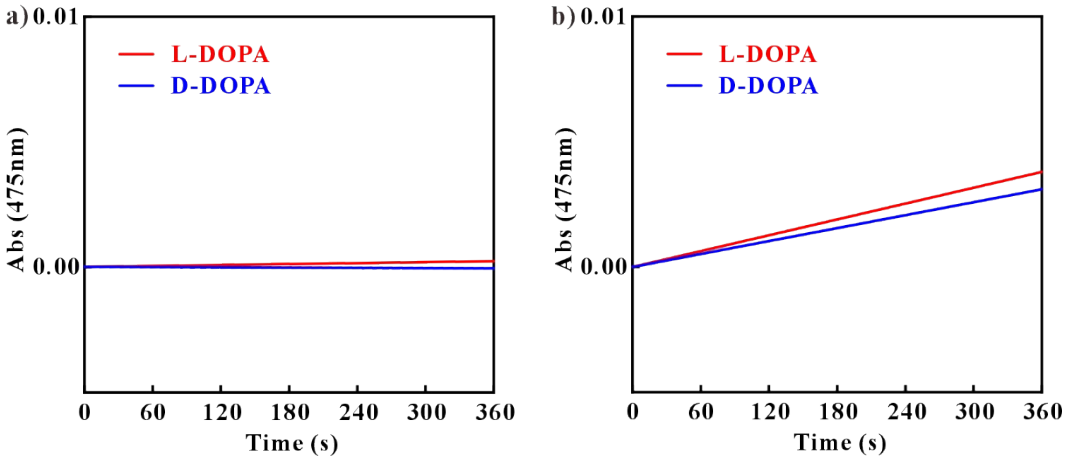

Fig. S21. The time-dependent absorbance changes at 475 nm for the L/D-DOPA oxidation catalyzed by the Co(II)-complexes of (a) **L-PhgC$_8$** and (b) **L-PhgC$_{12}$** in a 4/6 methanol/water solvent mixture. The concentration of L/D-DOPA was 2000 μM.

Table S3. Kinetic parameters for the catalytic oxidation of DOPA enantiomers by **(*P*)-D-PhgC$_{16}$-NR-M(II)**.

Sample	Substrate	K_M (μM)	K_{cat} (μM·s^{-1}·g^{-1})	K_{eff} (10^{-2} s^{-1}·g^{-1})	Select factor
(*P*)-D-PhgC$_{16}$-NR-Co(II)	***L*-DOPA**	195.2	13.25	6.79	2.80
	***D*-DOPA**	345.1	9.20	2.67	
(*P*)-D-PhgC$_{16}$-NR-Cu(II)	***L*-DOPA**	530.0	23.56	4.44	1.91
	***D*-DOPA**	637.3	14.73	2.35	
(*P*)-D-PhgC$_{16}$-NR-Mn(II)	***L*-DOPA**	342.1	10.90	3.19	1.86
	***D*-DOPA**	715.0	12.25	1.71	
(*P*)-D-PhgC$_{16}$-NR-Zn(II)	***L*-DOPA**	236.2	55.37	23.46	1.39
	***D*-DOPA**	317.1	53.44	16.88	

Table S4. Kinetic parameters for the catalytic oxidation of DOPA enantiomers by **(*M*)-L-PhgC$_{16}$-NR-M(II)**.

Sample	Substrate	K_M (μM)	K_{cat} (μM·s^{-1}·g^{-1})	K_{eff} (10^{-2} s^{-1}·g^{-1})	Select factor
(*M*)-L-PhgC$_{16}$-NR-Co(II)	***L*-DOPA**	481.2	15.26	3.17	
	***D*-DOPA**	228.1	17.02	7.47	2.35
(*M*)-L-PhgC$_{16}$-NR-Cu(II)	***L*-DOPA**	752.0	20.30	2.70	
	***D*-DOPA**	494.3	23.92	4.84	1.79
(*M*)-L-PhgC$_{16}$-NR-Mn(II)	***L*-DOPA**	706.0	12.63	1.79	
	***D*-DOPA**	449.1	14.00	3.12	1.74
(*M*)-L-PhgC$_{16}$-NR-Zn(II)	***L*-DOPA**	331.1	56.59	1.71	
	***D*-DOPA**	252.2	56.78	2.25	1.31

4.4 Catalytic cycles

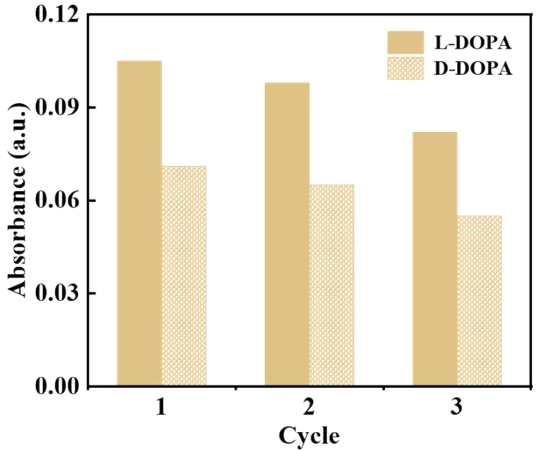

Fig. S22. The UV-vis absorbance performance of **(*P*)-D-PhgC$_{16}$-NR-Co(II)** catalyzing L/D-DOPA with three cycles.

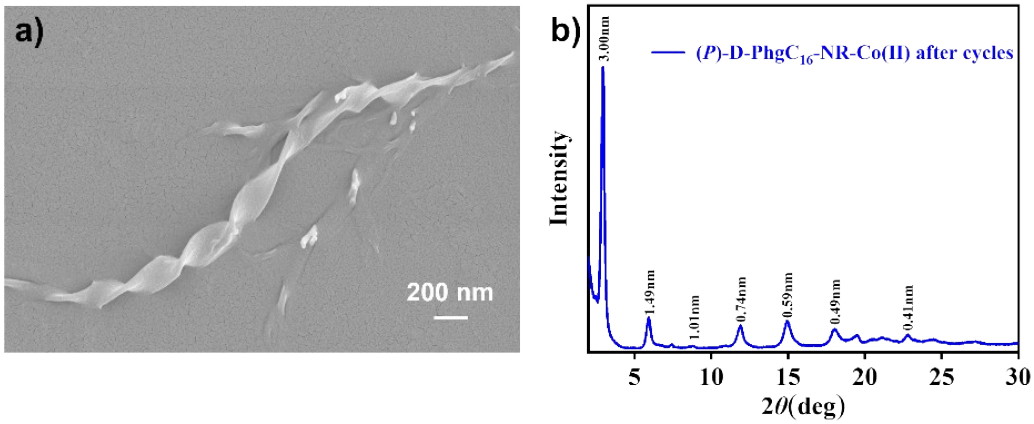

Fig. S23. a) SEM and (b) XRD patterns of **(*P*)-D-PhgC$_{16}$-NR-Co(II)** after three catalytic cycles.

4.5 pH effect

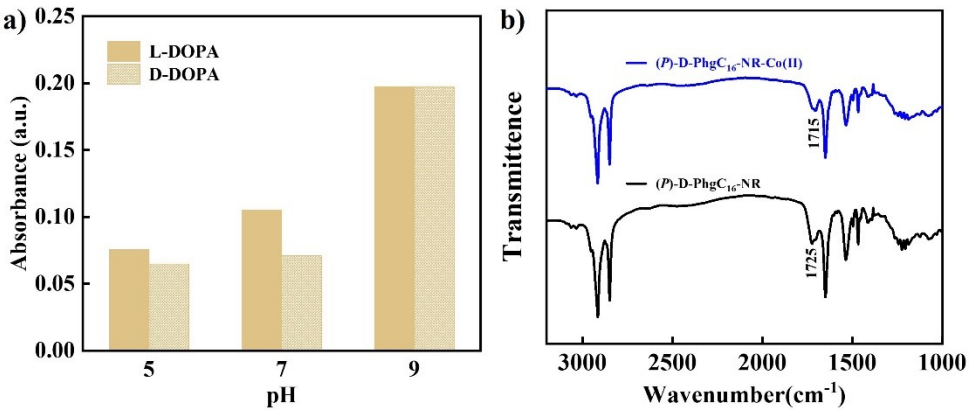

Fig. S24. a) The UV-vis absorbance performance of **(*P*)-D-PhgC$_{16}$-NR-Co(II)** catalyzing L/D-DOPA at different pH. (b) FTIR spectra of **(*P*)-D-PhgC$_{16}$-NR** (black line) and **(*P*)-D-PhgC$_{16}$-NR-Co(II)** (blue line) at pH 5.

Table S5. Comparison of the peroxidase-like catalytic enantioselectivity measured in our work with those reported in previous literatures.

Catalyst	Preferred substrate	Select factor	Reference
L-Cys@AuNPs-EMSN	D-DOPA	1.69	*Angew. Chem. Int. Ed.* **2018**, 57, 16791
D-Cys@AuNPs-EMSN	L-DOPA	1.47	
L-Cys@N-CuO/CoO NFs	D-DOPA	1.71	*Anal. Chem.* **2021**, 93, 11470
D-Cys@N-CuO/CoO NFs	L-DOPA	1.36	
D-His100@Fe-COF	D-DOPA	1.51	*Mater. Horiz.* **2020**, *7*, 3291
L-His100@Fe-COF	L-DOPA	1.86	
AuNP@LIPIA 1	D-DOPA	1.90	*Nanoscale* **2020**, *12*, 2422
AuNP@LIPIA 2	L-DOPA	1.1	
M-PANI-TA-Co^{2+}	D-DOPA	1.70	*Small* **2023**, DOI: 10.1002/smll.202303739
P-PANI-TA-Co^{2+}	L-DOPA	2.07	
(*M*)-L-PhgC_{16}-NR-Co(II)	D-DOPA	2.35	This work
(*P*)-D-PhgC_{16}-NR-Co(II)	L-DOPA	2.80	

5. Chirality transfer from (*P*/*M*)-D/L-PhgC$_{16}$-NR-M(II) to D/L-DOPA

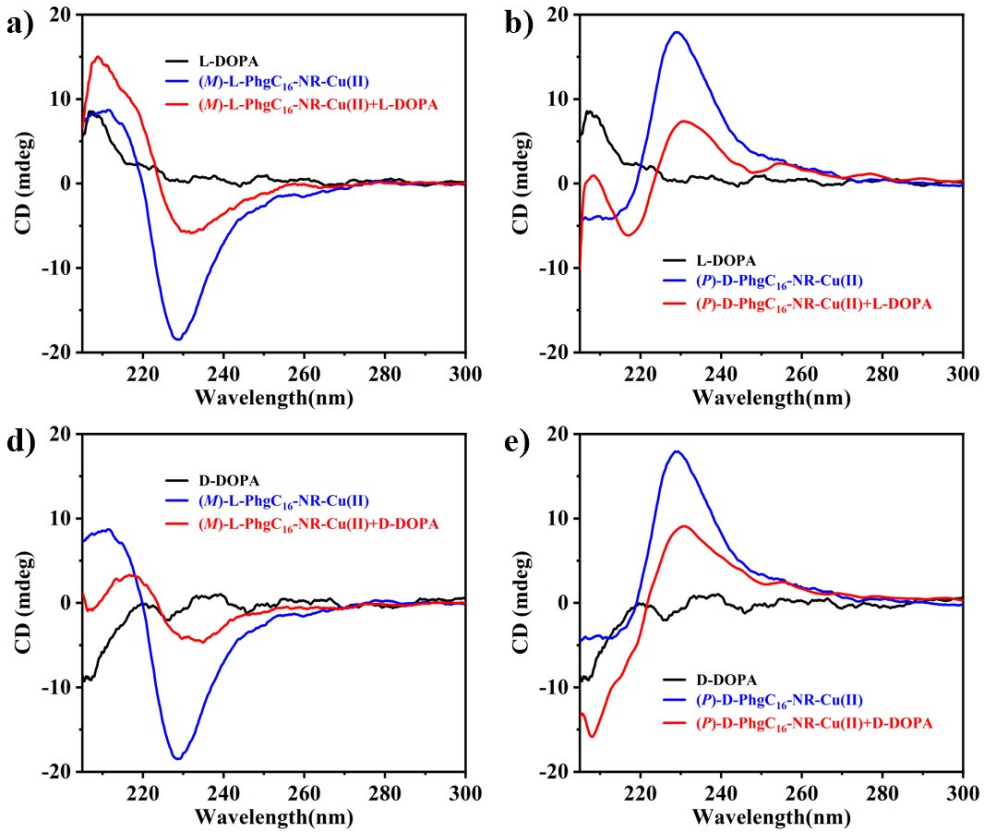

Fig. S25. CD spectra of **(*P*)-D-PhgC$_{16}$-NR** and **(*P*)-D-PhgC$_{16}$-NR-Cu(II)** ([Cu(II)/**D-PhgC$_{16}$** = 2.5%]) in the presence of a) D-DOPA and b) L-DOPA, as well as the CD spectra of **(*M*)-L-PhgC$_{16}$-NR** and **(*M*)-L-PhgC$_{16}$-NR-Cu(II)** ([Cu(II)/**L-PhgC$_{16}$** = 2.5%]) in the presence of c) D-DOPA and d) L-DOPA.

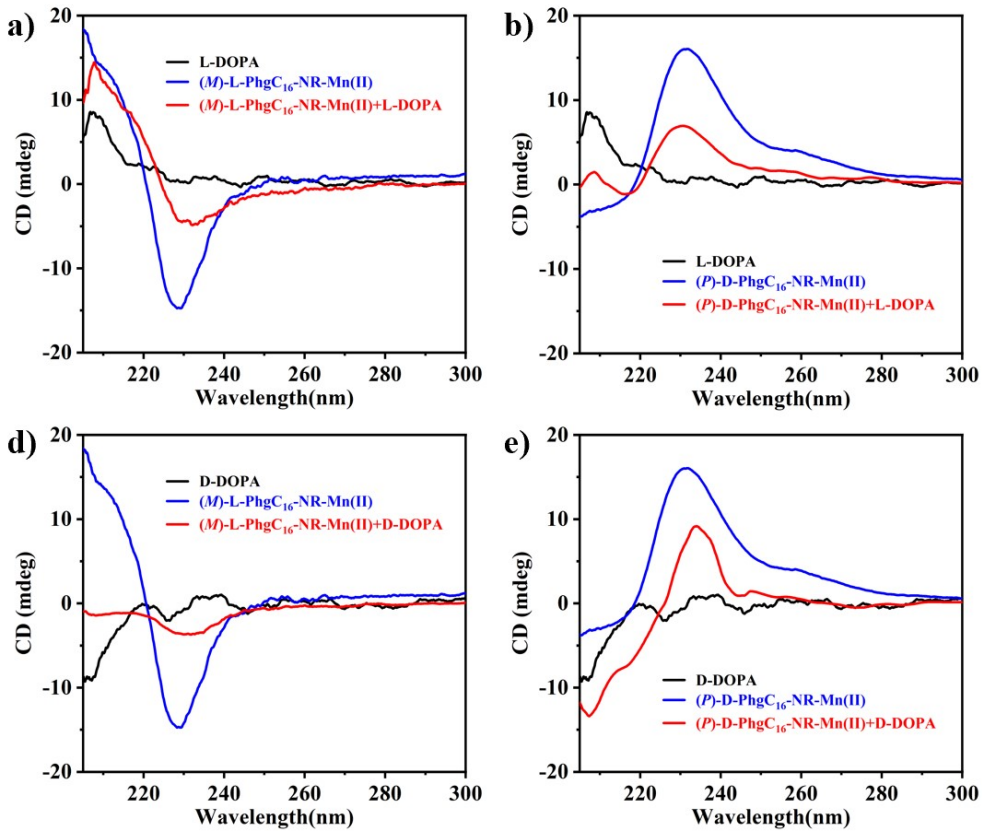

Fig. S26. CD spectra of **(*P*)-D-PhgC$_{16}$-NR** and **(*P*)-D-PhgC$_{16}$-NR-Mn(II)** ([Mn(II)/**D-PhgC$_{16}$** = 1.25%]) in the presence of a) D-DOPA and b) L-DOPA, as well as the CD spectra of **(*M*)-L-PhgC$_{16}$-NR** and **(*M*)-L-PhgC$_{16}$-NR-Mn(II)** ([Mn(II)/**L-PhgC$_{16}$** = 1.25%]) in the presence of c) D-DOPA and d) L-DOPA.

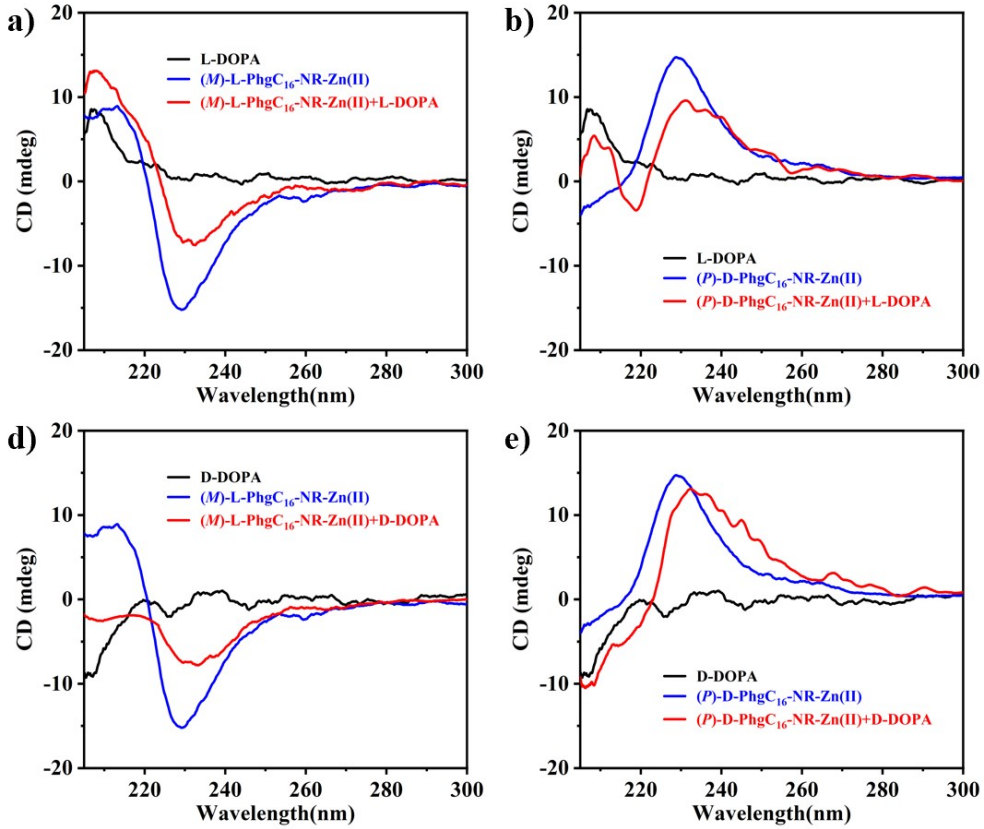

Fig. S27. CD spectra of **(*P*)-D-PhgC$_{16}$-NR** and **(*P*)-D-PhgC$_{16}$-NR-Zn(II)** ([Zn(II)/**D-PhgC$_{16}$** = 0.625%]) in the presence of a) D-DOPA and b) L-DOPA, as well as the CD spectra of **(*M*)-L-PhgC$_{16}$-NR** and **(*M*)-L-PhgC$_{16}$-NR-Zn(II)** ([Zn(II)/**L-PhgC$_{16}$** = 0.625%]) in the presence of c) D-DOPA and d) L-DOPA.

6. EPR analysis

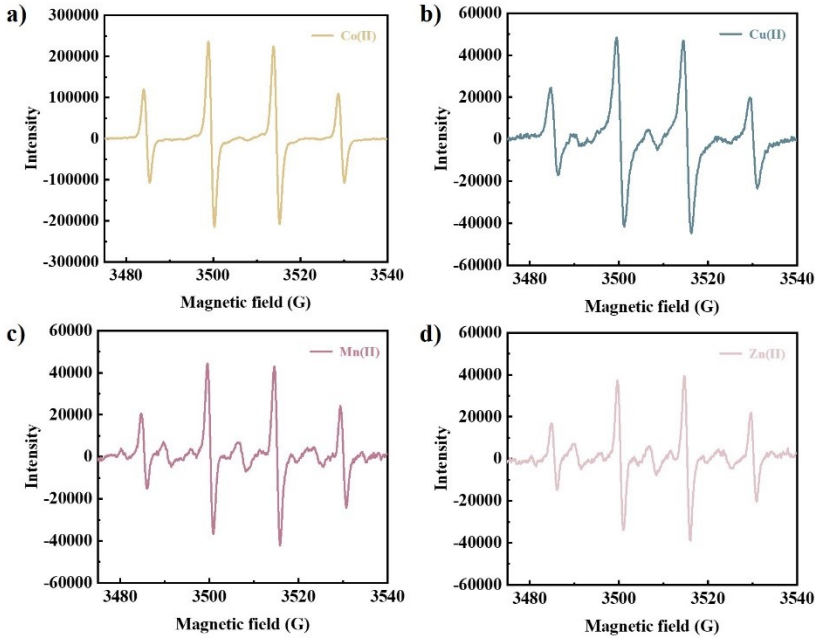

Fig. S28. EPR spectra for (a) Co(II), (b) Cu(II), (c) Mn(II), (d) Zn(II) in aqueous solution containing H_2O_2.

7. Binding affinity between (*P*)-D-PhgC$_{16}$-NR-Co(II) and DOPA enantiomers

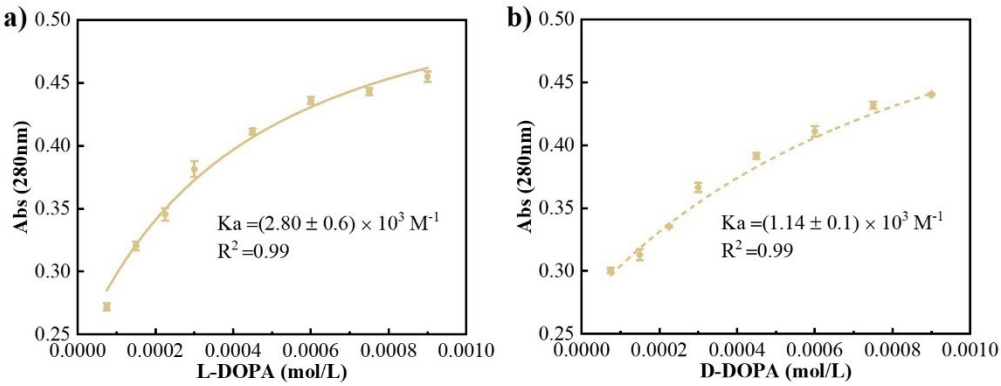

Fig. S29. Fit of UV titration experiments for **(*P*)-D-PhgC$_{16}$-NR-Co(II)** and a) L-DOPA and b) D-DOPA. The concentration of **(*P*)-D-PhgC$_{16}$-NR-Co(II)** was 50 μM. Error bars indicate standard deviations of two independent measurements.

8. References

[1] Chen, H.; Li, Y.; Tang, X.; Li, B.; Zhang, C.; Yang, Y., Preparation of single-handed helical carbonaceous nanotubes using 3-aminophenol-formaldehyde resin. *RSC Adv.* **2015,** *5* (50), 39946-39951.